16th World Conference on Earthquake Engineering, 16WCEE 2017

Santiago Chile, January 9th to 13th 2017

Paper N° 0256 (Abstract ID)

Registration Code: S-F1463217940

DEVELOPMENT OF A SEMI-ACTIVE FRICTION DAMPER FOR SEISMIC STRUCTURES BY USING LEVERAGE MECHANISM

L.-Y. Lu(1), S.-Y. Chu(2), H.-H. Wu(3) J.-R. Cheng(4)

(1) Professor, Dept. of Civil Engineering, National Cheng Kung University, Tainan, Taiwan, Email: lylu@mail.ncku.edu.tw
(2) Associate professor, Dept. of Civil Engineering, National Cheng Kung University, Taiwan, Email: sychu@mail.ncku.edu.tw.
(3) Taiwan, Graduate student, Dept. of Civil Engineering, National Cheng Kung University, Email: kshs970738@gmail.com.
(4) Master of Science, Dept. of Construction Engineering, National Kaohsiung First University of Sci. & Tech., Taiwan.

Abstract

For seismic protection of structural systems, a semi-active friction damper (SAFD) whose slip force is adjustable in real time, usually provides better control performance than that of a passive damper, since its damping force is adaptive to seismic excitation. However, traditional SAFDs are usually force-controlled devices, whose the slip force is varied by controlling the clamping force directly applied on the friction interface of the damper. Consequently, a huge clamping force has to be generated and the precise control of this force in real time may cause difficulty. To overcome this problem, a displacement-controlled SAFD, called a Leverage-type Controllable Friction Damper (LCFD) is proposed and studied experimentally in this study. The LCFD system consists of a traditional passive friction damper and a leverage mechanism with a movable central pivot (fulcrum). By adjusting the position of the pivot in real time, the equivalent friction force of the LCFD system can be controlled accurately without changing the damper clamping force. To verify the feasibility of this novel system, a prototype LCFD was installed in a single DOF seismic structure that was tested dynamically by using a shaking table. Both the experimental and theoretical results in this study have demonstrated that the friction damping force of the seismic structure with a LCFD can be varied in a desired manner through a displacement control method rather than a force control approach. It also demonstrated that, as compared with passive friction dampers, the energy dissipation capacity of the LCFD can be maximized in earthquakes of various intensity levels.

Keywords: leverage mechanism; friction damping; semi-active control; position control; energy dissipation device

1. Introduction

Among numerous structural control technologies that have been applied to protect structures from earthquake damage, seismic response modification using energy dissipation devices is the most widely adopted one. Friction dampers are one kind of energy dissipation devices and have been installed in numerous civil-engineering structures [1, 2]. Generally, a friction damper consists of one or more friction interfaces. A normal force is then applied to the interfaces to generate an energy-dissipating friction force when a seismic force is exerted on the structure where the damper is installed, consequently the damper will provide an additional energy dissipation mechanism for the structure [3]. This type of "passive" friction damper (PFD) does not require additional control energy to operate, and is thus easier to implement and more reliable. However, the internal parameters, such as the slip force, of a PFD are typically fixed values. In practice, the level of the slip force is predetermined according to the design earthquake load specified in a design code. Once the damper is designed and manufactured, the slip force may no longer be altered. This implies that the PFD cannot be adjusted in real time, in order to achieve better damping effect in an earthquake with intensity or characteristics that are different from the ones specified in the design code. For instance, a PFD may not be activated in a moderate earthquake, since its slip force is usually designed according to a strong earthquake. In other cases, a PFD may not exhibit sufficient capacity of energy dissipation under a severe earthquake, if its slip force is designed in an earthquake of lower intensity.

In response to the aforementioned drawbacks regarding PFDs, some researchers have conceived the idea of semi-active friction dampers (SAFDs) recently. Also called a variable or controllable friction damper, an SAFD is able to alter its friction force in real-time, according to the structural response or external excitation. In order to control the normal force on the friction interface of an SAFD, Kannan et al. [4] adopted a hydraulic power source able to generate huge actuation force, so a large variable friction force can be controlled. Yang and Agrawal [5] adopted an electromagnetic device to control the clamping force of an SAFD that is installed in an isolation system to enhance seismic safety of a building structure. Alternatively, numerous researchers have applied piezoelectric actuators to control the normal force of SAFDs [6-8]. Piezoelectric materials have the advantages of light weight, producing swift response and requiring minimum power source, etc. Laflamme et al. [9] and Cao et al. [10] incorporated drum brake components used in the automobile industry and hydraulic actuators to control the normal force of the SAFDs. Varela and Llera [11] proposed an SAFD design that used two-layer steel plates to increase the number of friction interfaces and a piezoelectric actuator to control the normal force. By increasing the friction-interface number, they intended to improve the force insufficiency typically exhibited in piezoelectric actuators.

As demonstrated in the studies mentioned previously, SAFDs generally are able to produce more favorable damping effects than that of PFDs because they are adaptive to seismic force characteristics and structural response. Moreover, like in active control, the application of SAFDs generally requires sensor deployment to instantaneously monitor the dynamic responses of the structural systems and also requires an on-line control law to determine the optimal friction force in real time. As a result, some studies have shown that the control effect of SAFDs may approach that of active control devices [7]. However, unlike active control devices, an SAFD does not require substantial control energy nor directly transfers control energy to the structure, making it more stable and reliable than active control systems.

As discussed previously, the friction forces of the SAFDs proposed in the previous works are primarily altered through directly controlling the normal forces of the SAFDs. This kind of semi-active dampers may be referred to as a force-controlled SAFD that generally require a large control force demand, since the controlled normal force may be several times of the desired slip force, depending on the material friction coefficient. The precise control over this large force may become difficult and expensive in real time. In view of this, the present study proposes a displacement-controlled SAFD called the leverage-type controllable friction damper (LCFD). This damper consists of a conventional PFD and a leverage mechanism with a movable central pivot. By controlling the pivot position on the lever-arm, the equivalent friction force of the LCFD can be altered instantaneously without changing the damper clamping force. The objective of the current study is to develop the theoretical basis for this novel semi-active friction system and to demonstrate its feasibility and adaptive nature by a shaking table test and numerical analysis.

2. Dynamic Equation of a Structure with a LCFD

2.1 Mathematical model

This section discusses the friction controllable concept of the proposed LCFD system. Fig. 1 illustrates the mathematical model of a structure equipped with the proposed LCFD that is installed on the first floor. Fig. 1 shows that the leverage mechanism includes a lever-arm with a movable central pivot (point P). One end of the lever-arm (point D) is connected to a brace that is then connected to the main structure. The effect of the brace stiffness, denoted by k_b, will be considered in the study. The other end of the lever-am (point A) is connected to a passive-type friction damper, whose friction force is expressed as u_f. The pivot point P can only move along the y axis, while point A and D can only move along the x axis. In the case where point P moves in the positive direction of the y axis (i.e., the pivot displacement $x_p > 0$), the length of the lever-arm at the damper end is larger than that at the structure end. As a result, the equivalent friction force $u(t)$ exerted on point D (the structural end) will be amplified, as compared with the actual friction force u_f (i.e., $u > u_f$). Conversely, when point P moves in the negative direction of the y axis (i.e., $x_p < 0$), the equivalent friction force exerted on the structure end will be reduced (i.e., $u < u_f$), since the lever-arm at the damper side is reduced. Therefore, the equivalent friction force $u(t)$ applied on the structure through the LCFD system can be controlled by changing the position of pivot point P, so that the goal of semi-active control can be achieved. Notably, although the leverage mechanism shown in Fig. 1 is depicted vertically for the convenience of explanation, in practice it may be placed horizontally for the convenience of installation.

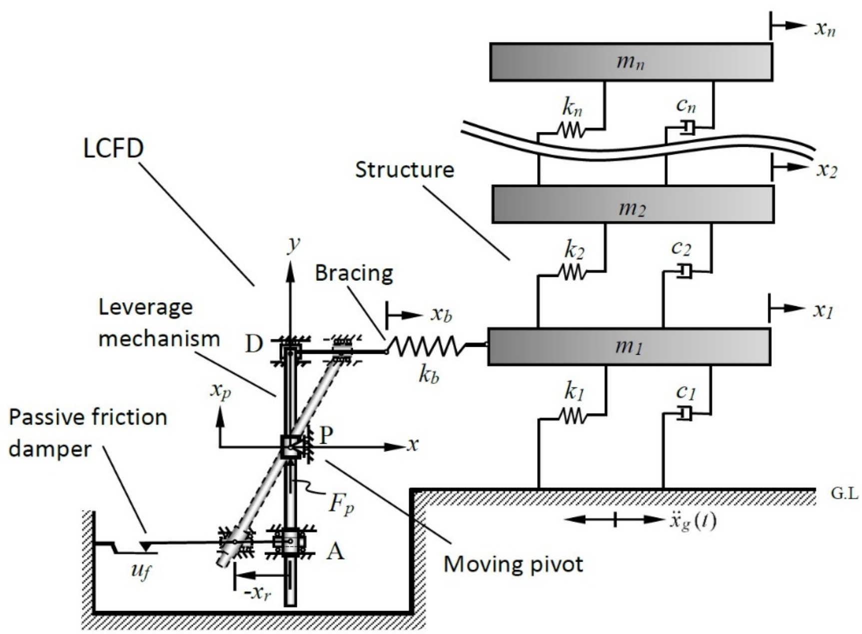

Fig. 1 – Mathematical model of a seismic structure with LCFD

2.2 Equation of motion

In this section, the equation of motion for an n-story shear-type structure with a LCFD will be discussed. The mathematical model of this structure is illustrated in Fig. 1, where x_i (i=1, 2,$\cdots n$) represents the relative-to-the-ground displacement of the structure in the i^{th} floor, m_i represents the mass of each floor, and $\ddot{x}_g$ denotes the ground acceleration. The symbols k_i and c_i (i=1, 2,$\cdots n$) represent the stiffness and damping coefficient of the i^{th} floor, and F_p represents the actuation force required to move the pivot point. In addition to the floor displacement x_i, the other degrees of freedom in Fig. 1 may also include the pivot displacement x_p, friction damper stroke x_r, and bracing deformation x_b. For the mathematical model illustrated in Fig. 1, there are totally (n+2) independent degrees of freedom, i.e., x_b, x_p, and x_i (i=1, 2,$\cdots n$) in the system. From Fig. 1, it should be clear that the LCFD can also to placed on any story other than the first story.

After knowing each of the degrees of freedom, the equations of motion for the model shown in Fig. 1 may be derived by using the Lagrange's equation of motion. The derivation will lead to the following matrix equation.

$$\mathbf{M}_s \ddot{\mathbf{x}}(t) + \mathbf{C}_s \dot{\mathbf{x}}(t) + \mathbf{K}_s \mathbf{x}(t) = \mathbf{B}_s (-u(t)) - \mathbf{E}_s \ddot{x}_g(t) \tag{1}$$

where matrices $\mathbf{M}_s$, $\mathbf{C}_s$, and $\mathbf{K}_s$, whose dimensions are (n×n), represent the structural mass, damping and stiffness matrices, respectively. Moreover, $\mathbf{x}(t)$ represents the displacement vector that contains x_i (i=1, 2,$\cdots n$); $\mathbf{B}_s$ represents the damper placement matrix; $\mathbf{E}_s$ represents the seismic force distribution matrix. In Eq. (1), the term $u(t)$, called the semi-active friction force of the LCFD, physically represents the equivalent friction force exerted on the structure end. This semi-active force can be written as

$$u(t) = -r_p(t) u_f(\mathrm{t}) \tag{2}$$

$$r_p(t) = \frac{L + 2x_p(t)}{L - 2x_p(t)} \tag{3}$$

where $r_p(t)$ denotes the leverage amplification factor, which is dimensionless and associated with the pivot position $x_p(t)$. Eq. (2) states that because of $r_p(t)$, the passive damper friction force $u_f(t)$ is converted to a controllable friction force $u(t)$. Notably, if x_p is within the range of $-0.5L \le x_p \le 0.5L$, then $r_p(t)$ in Eq. (3) is always positive (i.e., $r_p(t) \ge 0$). In view of Eqs. (2) and (3), the semi-active friction force $u(t)$ is controllable by adjusting the pivot position $x_p(t)$, which is generally determined in real-time by a prescribed control law. Furthermore, the Lagrange's equation in the degree of freedom of $x_p(t)$ may also lead to the following equation

$$F_p(t) = (x_b(t) - x_1(t)) \left[\frac{4Lu_f(t)}{(L - 2x_p(t))^2} \right] = \frac{(x_b(t) - x_1(t))}{L} \left[\frac{4\,u_f(t)}{(1 - \frac{2x_p(t)}{L})^2} \right] \tag{4}$$

where $F_p(t)$ denotes the required control force to drive the piovt P to the desired loaction $x_p(t)$. The last equation states that the magnitude of the driving force $F_p(t)$ actually depends on several variables, including the pivot displacement x_p, bracing deformation x_b, displacement of the first floor x_1, and damper passive friction u_f. The equation also shows that F_p is inversely proportional to the lever-arm length L.

3. Prototype LCFD

To verify the LCFD theory developed previously, a prototype LCFD system was designed and manufactured in the present study, and a shaking table test was conducted for the prototype system. A photo of the prototype system is shown in Fig. 2, and the specifications of the system are tabulated in Table 1. As shown in Fig 2, the prototype can be largely divided into four parts: (1) sliding frame, (2) leverage system, (3) passive friction damper (PFD), and (4) driving and control system (pivot position control system). A detailed description for each part and corresponding function are presented below.

(1) **Sliding frame** is primarily used to simulate a single-DOF structural system. The sliding frame comprises springs, a bracing device and guide rails. The springs are used to simulate the stiffness and restoring force provided by the structure itself. The bracing device, connected between the lever-arm and the frame, is used to mimic the stiffness effect of the bracing (see Fig. 1). The low-friction guide rails restraint the movement of the structure in horizontal direction. The sliding frame will be loaded with mass blocks to simulate the structural mass.

(2) **Leverage system** comprises a lever-arm with a central pivot (point P) that moves along the lever y-axis. As illustrated in Fig. 1, the lever-arm is subsequently joined to point D and point A on the two ends. Point D is connected to the sliding frame via the bracing spring, while point A is joined to the PFD via a linear bearing. The moving directions of points D and A must be parallel to that of the sliding frame, while perpendicular to that of point P.

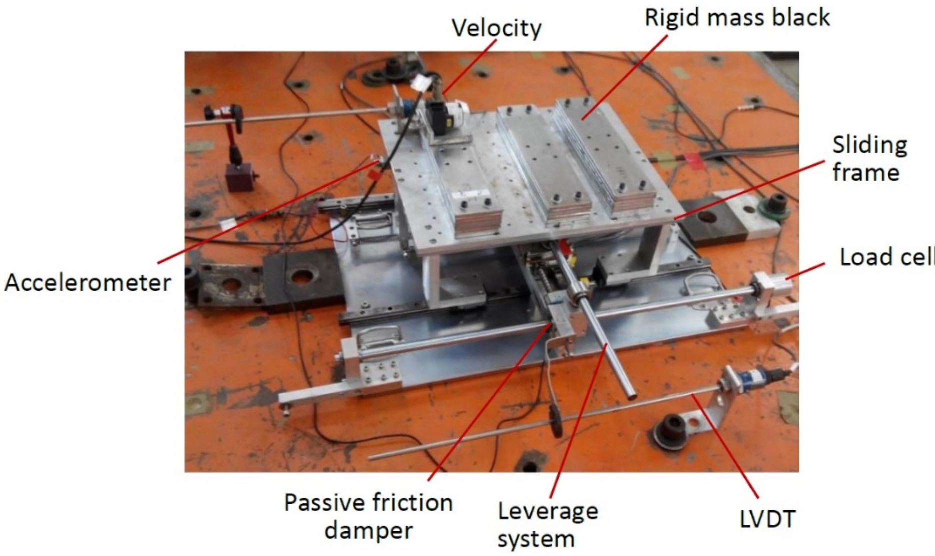

Fig. 2 – Photo of the prototype LCFD and test setup

(3) **PFD** is used to generate a constant slip force, which is then transferred through the leverage system to the structure (the sliding frame) to produce a controllable friction force. The PFD primarily comprises a pre-compression screw, friction pads, and friction bar. The friction pads are made of brass, which is one kind of materials with stable friction property. The pre-compression screw exerts a normal force between the friction pads and friction bar, and will produce a stable friction force when a relative motion occurs between the friction pads and bar. This friction damping force is transferred to the sliding frame via the lever-arm.

(4) **Driving and control system**, which is primarily used to control the position of the moving pivot P on the lever-arm, consists of a lead screw set, servo motor, motor controller box, analog-to-digital motion card (A/D card), personal computer (PC) and sensors. The on-line control command of the pivot displacement is first computed by the PC, based on the sensor feedback signal, and transmitted to the motor controller box through the motion card, and then the servo motor and lead screw set will drive the pivot P to the designated position decided by the control law.

4. Control Law-Proportional Displacement Control

In order to effectively suppress structural vibrations, a suitable control law is required to determine the pivot position of the prototype LCFD. Since the LCFD is one kind of semi-active control hardware, many possible controllers may be adopted for the LCFD. Nevertheless, as mentioned previously, the objective of this study is to develop a novel semi-active system and to demonstrate physically its feasibility and adaptive nature. To focus on this objective rather than the control law, a simple controller is adopted in the test. The controller, called the proportional displacement control (PDC), is developed based on the assumption that an increased story drift of the structure usually implies an increased seismic force exerted on the structure. Thus, the LCFD should generate a larger friction force to suppress the structural response when the story drift increases. Conversely, a decreased story drift represents a decreased seismic force, and thus only a smaller friction force is required. Under this assumption, the PDC intends to maintain a direct proportionality between the equivalent friction $u(t)$ of the LCFD and the story drift. As a result, the PDC only requires the measurement of the story drift of the structure, and thus is convenient and easy to implement.

As indicated in Eq. (2), the LCFD is able to convert the passive friction u_f into the semi-active friction force u by adjusting the leverage amplification factor r_p. Therefore, in order to realize the concept of the PDC explained above, the relation between the factor $r_p(t)$ and story drift $x_1(t)$ is depicted in Fig. 3, where $r_{p,max}$ and $r_{p,min}$ denote the upper and lower bounds of r_p and $x_{1,max}$ represents a threshold value of $x_1(t)$ at which r_p reaches its upper bound $r_{p,max}$. As illustrated in Fig. 3, the PDC will change the value of r_p within the lower bound $r_{p,min}$ and upper bound $r_{p,max}$, while the slope s of the change will be determined by the threshold value of $x_{1,max}$. Therefore, PDC comprises three controller parameters, $r_{p,max}$, $r_{p,min}$, and $x_{1,max}$, which have to be determined by the designer. In practice, the value of $r_{p,min}$ aims to mitigate the structural response in a small to medium earthquake, while the value of $r_{p,max}$ is desinated to suppress the structural response of a strong to sever earthquake. Once the on-line value of $r_p(t)$ is determined by the PDC, Eq. (3) can be used to solve the required pivot position $x_p(t)$ for the desired value of $r_p(t)$, as shown below

$$x_p(t) = \frac{L(\hat{r}_p(t)-1)}{2(\hat{r}_p(t)+1)} \tag{5}$$

where $\hat{r}_p(t)$ denotes the value determined by the PDC controller.

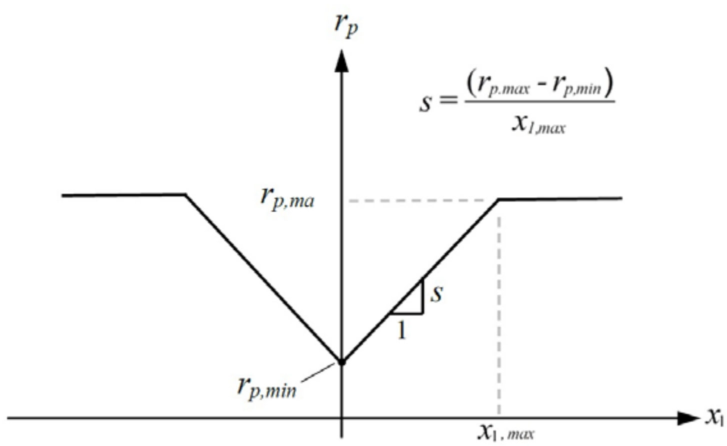

Fig. 3 – Relationship of r_p and x_1 given by the PDC controller

5. Experimental Verification by Shaking Table Test

5.1 Test setup and system parameters

In the shaking table test of this study, a simple structure with one degree of freedom was tested, so that the characteristics of the LCFD system itself under seismic excitation can be observed more clearly. The test setup was already illustrated in Fig. 2, while the system parameters of the LCFD specimen are tabulated in Table 1. This LCFD-controlled single-DOF structure can be modelled by Fig. 1 by letting $n = 1$. The parametric values listed in Table 1 were identified from a component test on the prototype LCFD conducted prior to the shaking table test. As shown in the table, the controlled structure has a natural period of 1 Hz. The total structural mass m_1 is 59 kg, which is the sum of the mass of sliding frame (38 kg) and added mass blocks (21 kg). The friction coefficient of the guide rails is about 0.026 which leads to an equivalent structural damping ratio of about 2.9%. In addition, the bracing stiffness was taken to be about 21.2 times of the structural stiffness, i.e., $k_b = 21.2k_1$. Moreover, the total slip force of the PFD was about $u_{f,\max}$ =0.092 $(m_1 g)$, where $(m_1 g)$ denotes the total structural weight. The length L of the lever-arm is 0.38 m, and the pivot stroke of point P is x_p = ±0.087 m that is about ±0.21L. Also shown in Table 1, the upper and lower bounds of r_p for the PDC controller were chosen to be 2.4 and 0.5, respectively, while the threshold displacement $x_{1,max}$ was taken to be 0.125m. These values are determined by a parametric study under the physical restraints of the prototype LCFD, such as the speed of the servo-motor. In the parametric study, the 1940 El Centro Earthquake was used as the excitation. The sensor deployment is also shown in Fig. 2. As shown, a displacement meter (LVDT) and accelerometer were installed on the sliding frame to measure the story drift of the controlled structure. A load cell and displacement meter were installed inside the LCFD to measure the variation of the semi-active friction force u and pivot displacement x_p, respectively. Additional two load cells were installed to measure the passive friction force u_f (see Fig. 2) and the normal force N of the PFD. A displacement meter was also installed on the PFD to record the movement x_r of the damper.

Table 1 – Parametric values of the prototype LCFD

System	Item	Parameter
Primary structure	Mass (m_1)	59 kg
	Damping coeff. (c_1)	21.673 N/(m/s)
	Equivalent damping ratio (ζ_1)	2.9 %
	Stiffness (k_1)	2317.210 N/m
	Natural freq. (ω_1)	1 Hz
	Bracing stiffness (k_b)	49143 N/m
	Friction coeff. of guide rails (u_i)	0.026
LCFD	Slip force of friction damper ($u_{f,max}$)	45.6N (= 0.076 m_1 g)
	Length of lever-arm (L)	0.38 m
	Range of pivot displacement ($x_{p,max}$, $x_{p,min}$)	(0.21L, -0.21L) m
PDC controller	Range of r_p ($r_{p,max}$, $r_{p,min}$)	(2.4, 0.5)
	Threshold structural disp. ($x_{1,max}$)	0.125 m

5.2 Comparison between experimental and theoretical results

In order to verify the analysis method developed in the previous sections, the experimental and simulated responses of the LCFD with the PDC controller subjected to the El Centro earthquake are compared in Fig. 4. The comparisons of time-history responses of the relative displacement (story drift) and structural acceleration are depicted in Fig. 4(a) and 4(b), respectively. An observation on both figures shows that the dynamic behavior and trends of the displacement and acceleration responses of the tested LCFD match very well with those of the simulated ones, with only slight differences in peak values and residual displacement. The result suggests that the proposed analytical model is able to accurately simulate the dynamic behavior of a LCFD-controlled structure.

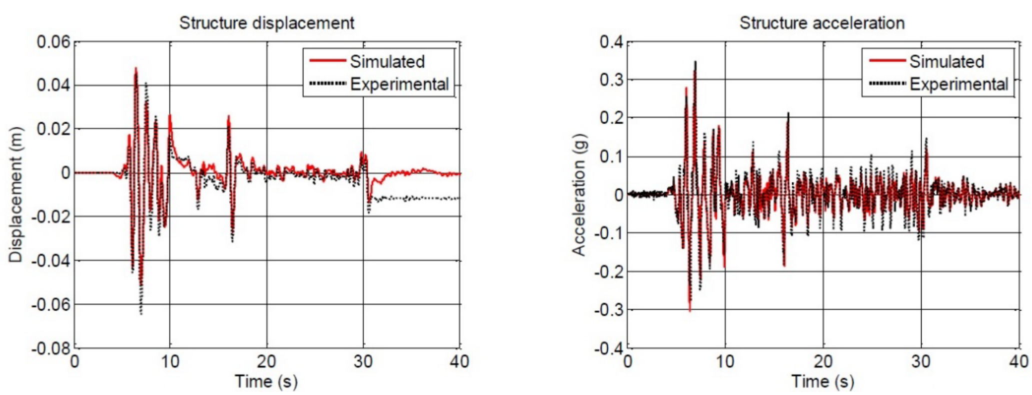

(a) Story drift (b) Structural acceleration

Fig. 4 – Time history of LCFD responses (El Centro earthquake, PGA=0.4g)

Moreover, under the El Centro earthquake, Fig. 5(a) compares the experimental and numerical hysteresis loops (u_f vs. x_r) at the passive damper end (point A), while Fig. 5(b) compares the hysteresis loop of the semi-active friction force (u vs. x_1) at the structural end (point D). As expected, Fig. 5(a) shows that the hysteresis loop of the passive PFD is rectangular with a constant slip force, and the figure also reveals that the cyclic friction behavior of the PFD is relatively stable. This reveals that the friction property of the PFD is consistent with the Coulomb friction model employed in the numerical analysis. Unlike the loop shown in Fig. 5(a), Fig. 5(b) demonstrates that the hysteretic loop of the semi-active friction force at the structural end is no longer a rectangle but becomes two trapezoids. The slip force in this trapezoidal hysteresis loop increases proportionally along with the increase of structure displacement. This highlights that the pivot position of the LCFD was effectively shifted by the PDC controller, so that the equivalent hysteretic behavior of the friction damper is altered in a desired manner. The results of Fig. 5 further confirm that the friction damping force of the LCFD can be effectively controlled by changing the pivot position.

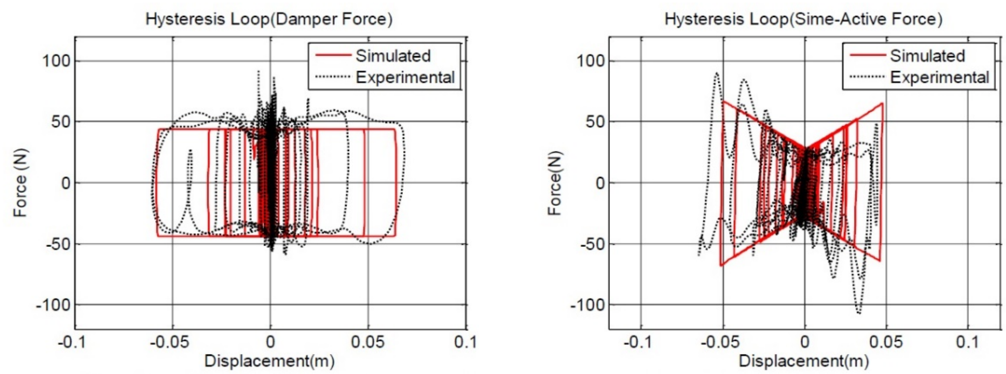

(a) Passive friction force (u_f vs. x_r) (b) Semi-active friction force (u vs. x_1)

Fig. 5 – Comparison of hysteresis loops of LCFD (El Centro earthquake, PGA=0.4g)

6. Energy Dissipated by LCFD

To further highlight the adaptive nature of the LCFD system, this section compared the simulated response of the LCFD(PDC) with those of two other passive control schemes, namely, Passive-max and Passive-min. In Passive-max, the pivot position of the LCFD is fixed at the upper bound of r_p of PDC (i.e., $r_p = r_{p,\max}$); whereas in Passive-min, the lever pivot position is fixed at the lower bound r_p (i.e., $r_p = r_{p,\min}$). In this section, all responses are simulated by using the numerical model described previously. In the simulation, the lower and upper bounds of r_p in this study are taken to be $r_{p,\min} = 0.5$ and $r_{p,\max} = 2.4$, respectively, while the critical displacement is taken to be $x_{1,\max} = 0.05$ m.

Under the Newhall earthquake, Fig. 6 compares the hysteresis loops of the LCFD with the three control cases, namely, PDC, Passive-max and Passive-min controls. Two PGA levels, i.e., 0.1g and 0.6g, are considered in the figure. PGA=0.1g is meant to represents an earthquake with small intensity, while PGA=0.6g represents a severe earthquake. Fig. 7 compares the time histories of the accumulative energy dissipated by the three control cases for the two different earthquake intensities. Note that the energy dissipation at a given time instant $E_u(t)$ in Fig. 7 is calculated by using the following equation

$$E_u(t) = \int_0^t u(\tau)\, dx_D(\tau) \tag{6}$$

where $x_D(t)$ denotes the relative displacement of point D in Fig. 1. Figures 6(a) reveals that in the small earthquake (PGA=0.1g) the hysteresis loop of the PDC controller is closer to that of the Passive-min; while Fig. 7(a) shows that the PDC and Passive-min dissipate almost the same amount of seismic energy and is much larger than that of the Passive-max, since the friction damper in the Passive-max was not activated during the most of earthquake duration. On the other hand, in a severe earthquake (PGA=0.6g), Fig. 6(b) shows that the loop of the

PDC is enlarged and dissipates much more energy than that of the Passive-min. Fig. 7(b) indicates that the amount of energy dissipated by the PDC at PGA=0.6g is much larger than that of the Passive-min, and is even larger than that of the Passive-max. Therefore, Figs. 6 and 7 together have demonstrated the superior adaptability of the LCFD with the PDC controller. Notably, although in Fig. 6(a) the Passive-max seems to have least story drift, it also exerts the highest force on the structure, which could lead to a higher structural acceleration. More detailed results about the acceleration response of a LCFD-controlled structure were given in Ref. [12].

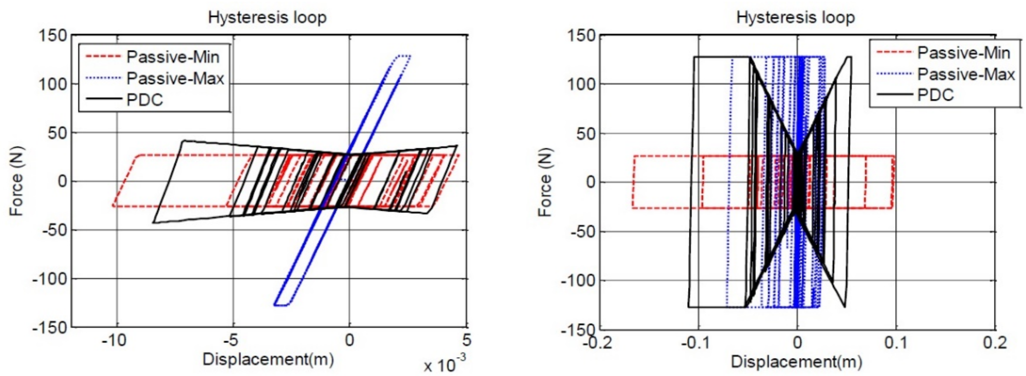

(a) PGA=0.1g (b) PGA=0.6g

Fig. 6 – Comparison of hysteresis loops of LCFD with three control cases (Newhall earthquake)

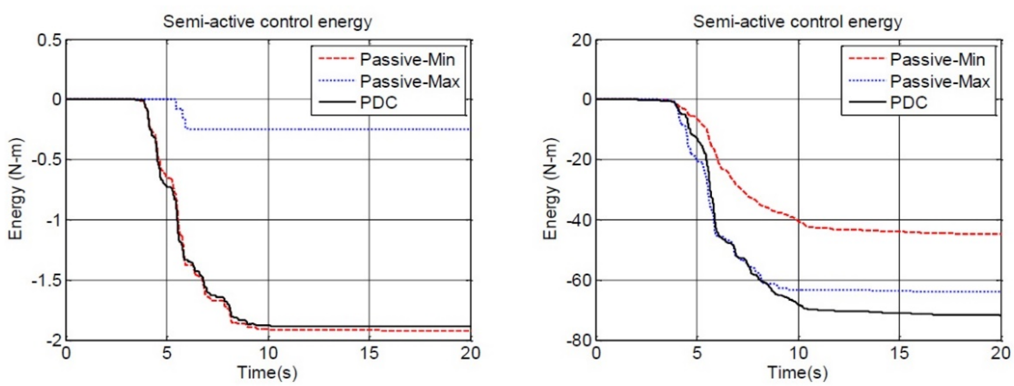

(a) PGA=0.1g (b) PGA=0.6g

Fig. 7 – Comparison of dissipated energy of LCFD with three control cases
($x_{1,\max} = 0.05$ m, Newhall earthquake)

7. CONCLUSIONS

A semi-active friction damper (SAFD) may provide better seismic protection for a structural system than a passive damper, since its damping force is controllable in real time. However, a conventional SAFD usually employs a force control method to regulate the clamping force on the friction interface. Consequently, this may lead a demand on the precise control of a huge force. To avert this problem, the notion of leverage-type controllable friction damper (LCFD) is proposed and its feasibility is verified experimentally in this study. Different from traditional SAFDs, the LCFD regulates its friction damping force by a displacement control approach. An LCFD is primarily composed of a passive friction damper and a leverage mechanism with a movable central pivot. By controlling the pivot position in real time, the effective friction force of the LCFD system can be adjusted precisely. The analytical model and governing equation for a structure with the LCFD were first discussed in this study. To verify the analytical model, a prototype system was fabricated and tested dynamically by using an earthquake simulator (shaking table). Moreover, in order to determine the pivot position effectively, a simple control law called “proportional displacement control (PDC)” was adopted in the test. The goal of the PDC is to make the effective friction force of the LCFD proportional to the story drift of the controlled structure, such that the LCFD will have a smaller damping force in an earthquake of lower intensity, while a larger damping force in a severe earthquake. The PDC merely requires the feedback of the story drift, and thus is extremely easy to implement.

The test result has demonstrated that the PDC controller is able to alter the hysteresis loop and energy dissipation performance of the LCFD in a desired manner. The test also produced consistent results between experimental and numerical data. This not only verifies the analytical model developed in this study, but also confirms the feasibility of the LCFD technology. Finally, a numerical investigation into energy dissipation capacity of the LCFD further demonstrates the advantage and adaptability of the system. The PDC enables the LCFD in a structure to exhibit smaller slip force when experiencing a smaller earthquake, such that the friction damper in the LCFD will remain activated and dissipate more seismic energy. Conversely, when experiencing a larger ground motion, the LCFD will exhibit a larger slip force, such that a more seismic energy can be dissipated.

8. Acknowledgement

This research was supported in part by the Ministry of Science and Technology of R.O.C. (Taiwan), through grant MOST103-2625-M-006-010. The authors are grateful to the Department of Construction Engineering, National Kaohsiung First University of Science and Technology for their technical support in conducting the shaking table test.

9. References

[1] Pall RT, Gauthier G, Delisle S and Pall A (2000): Friction-dampers for seismic upgrade police headquarters, Montreal. *Proceedings of the 12th World Conferences on Earthquake Engineering*, New Zealand, paper no. 2014.

[2] Pasquin C, Charania H, Steele R, Pall R and Pall A (1998): Friction-dampers for seismic control of Selkirk Water *Front* Offices, Victoria. *The 6th U.S. National Conference on Earthquake Engineering*, Sheraton Seattle Hotel, Seattle, Washington.

[3] Soong TT and Spencer BF (2002): Supplemental energy dissipation: state-of-the-art and state-of-the practice. *Engineering Structures*, 24: 243-259.

[4] Kannan S, Uras HM, Aktan HM (1995): Active control of building seismic response by energy dissipation. *Earthquake Engineering and Structural Dynamics*, 24(5):747-759.

[5] Yang JN, Agrawal AK (2002): Semi-active hybrid control systems for nonlinear building against near-fault earthquakes. *Engineering Structures*, 24(3): 271-280.

[6] Lu LY, Lin CC, Lin GL, Lin CY (2010): Experiment and analysis of a fuzzy-controlled piezoelectric seismic isolation system. *Journal of Sound and Vibration*, 329(11): 1992-2014.

[7] Lu LY, Lin GL, Lin CY (2011): Experimental verification of a piezoelectric smart isolation system. *Structural Control and Health Monitoring*, 18(8): 869-889.

[8] Ozbulut E, Bitaraf M (2011): Adaptive control of base-isolated structures against near-field earthquakes using variable friction dampers. *Engineering Structures*, 33:3143-3154.

[9] Laflamme M, Taylor D, Abdellaoui Maane M., Connor JJ (2012): Modified friction device for control of large-scale systems. *Structural Control and Health Monitoring*, 19(4):548-564.

[10] Cao L, Downey A, Laflamme S, Taylor D, Ricles J (2015): Variable friction device for structural control based on duo-servo vehicle brake: Modeling and experimental validation. *Journal of Sound a*nd Vibration, 348:41-56.

[11] Varela JP, Llera JC (2015): A Semi-active piezoelectric friction damper. *Earthquake Engineering and* Structure *Dynamics*, 44:333-534.

[12] Cheng JR (2015): *Development of a leverage-type semi-active friction damper for seismic response mitigation of structures*. Master thesis, National Kaohsiung First University of Science and Technology.